Chapter 5

Mathematical Model of Excavator Digging

Chapter 5

Mathematical Model of Excavator Digging

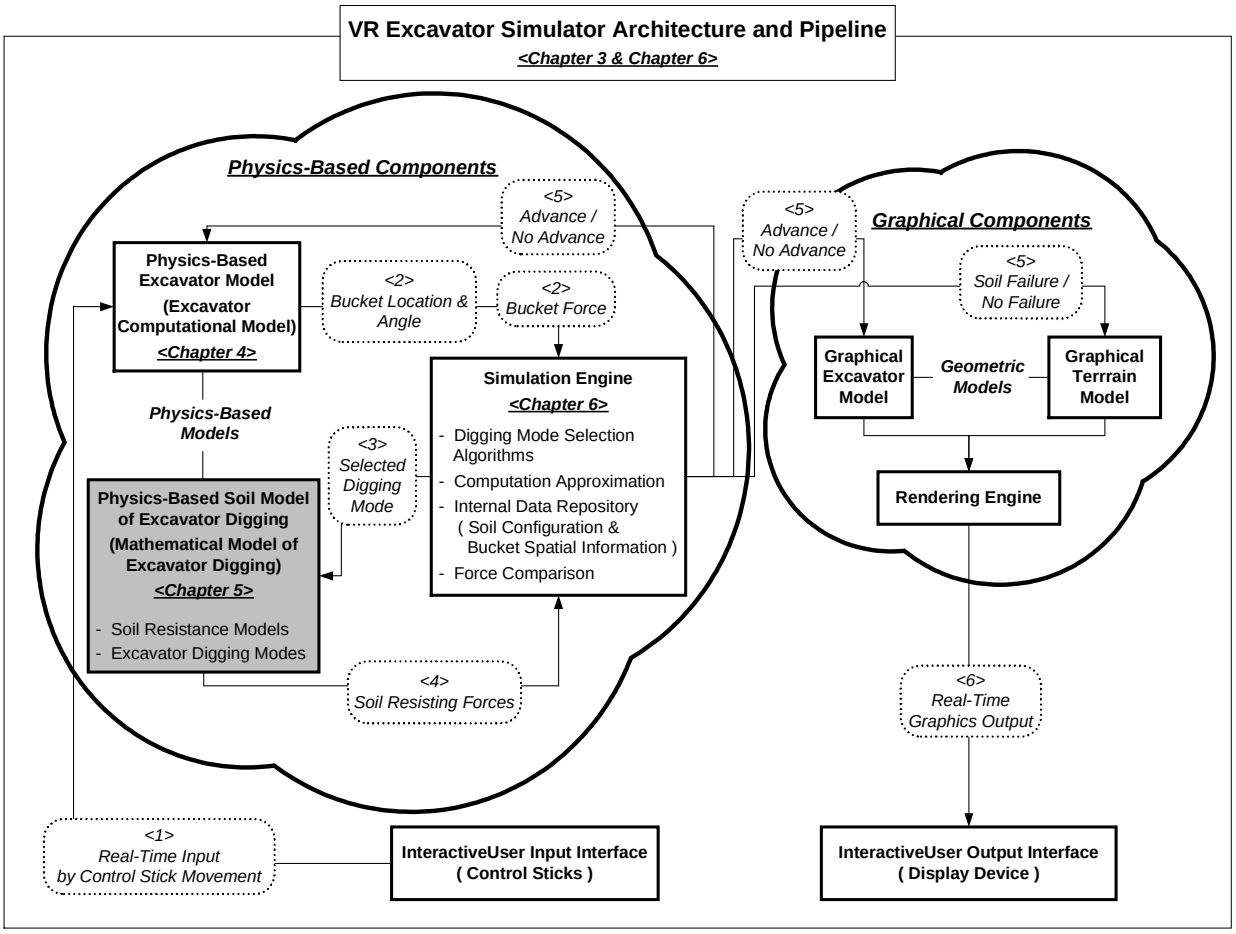

5.1 Introduction

As depicted in the VR excavator simulator architecture, the mathematical model of excavator digging (or physics-based soil model of excavator digging) functions as an external medium to regulate the behavior of an excavator. Specifically it provides soil resistance forces to the excavator computational model (or physics-based excavator model) through the simulation engine so that physically valid movement of a bucket through soil medium is achieved.

Three different digging mechanisms (penetration, separation, and secondary separation) are identified in Chapter 2 as the basic instruments to explain soil failure induced by an excavator digging tool.

In this chapter, we begin by analyzing an excavator digging tool, a bucket, to determine which bucket area or areas are accountable for particular digging mechanisms (Section 5.2). The identified bucket areas accounting for a particular mechanism are grouped together to form an idealized bucket part. These parts make up an idealized bucket.

Using the idealized bucket, a partially-competent separation model and a general purpose penetration theory, two soil resistance models for excavator digging are developed to predict a penetration-based resistance and a separation-based resistance to the digging tool (Section 5.3 and 5.4).

The one-mechanism-based soil resistance models are joined together to form a complete mathematical model of excavator digging through the use of different excavator digging modes (Section 5.5). Criteria to differentiate one digging mode from another are described along with typical situational digging operations.

5.2 Idealized Excavator Bucket

Different types of buckets used in construction excavation are shown in Figure 5.1. To avoid extra complexity of bucket-soil interaction in mathematical modeling, it is necessary to simplify the shape of a typical bucket.

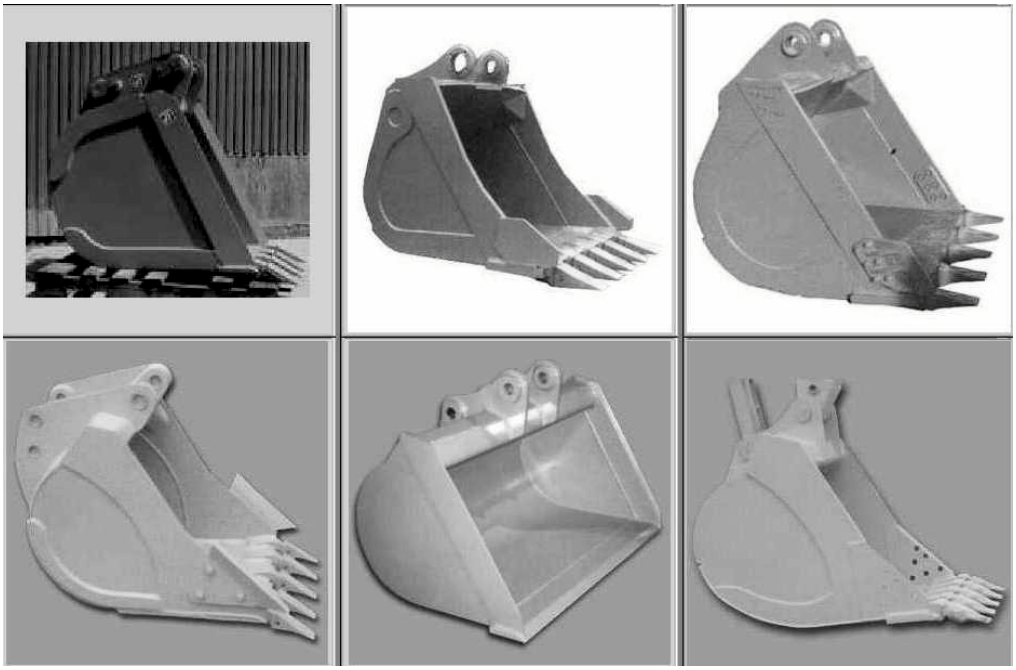

Figure 5.1 Various Excavator Buckets Used in Construction

The steps in transforming an excavator bucket into an idealized bucket are depicted in the diagrams of Figure 5.2 through Figure 5.4. This transformation is based on the assumption that an excavator bucket relies on its penetration, and primary and secondary separation forces for breaking soil. Therefore, the idealized bucket should have parts generating these forces. The detailed description on the breakdown of each of the separation and penetration forces into componential forces is continued in the later sections.

As shown in Figure 5.2, a typical bucket is comprised of 1) *teeth, 2) a bottom plate,* and 3) *a convex plate* and *side plates*.

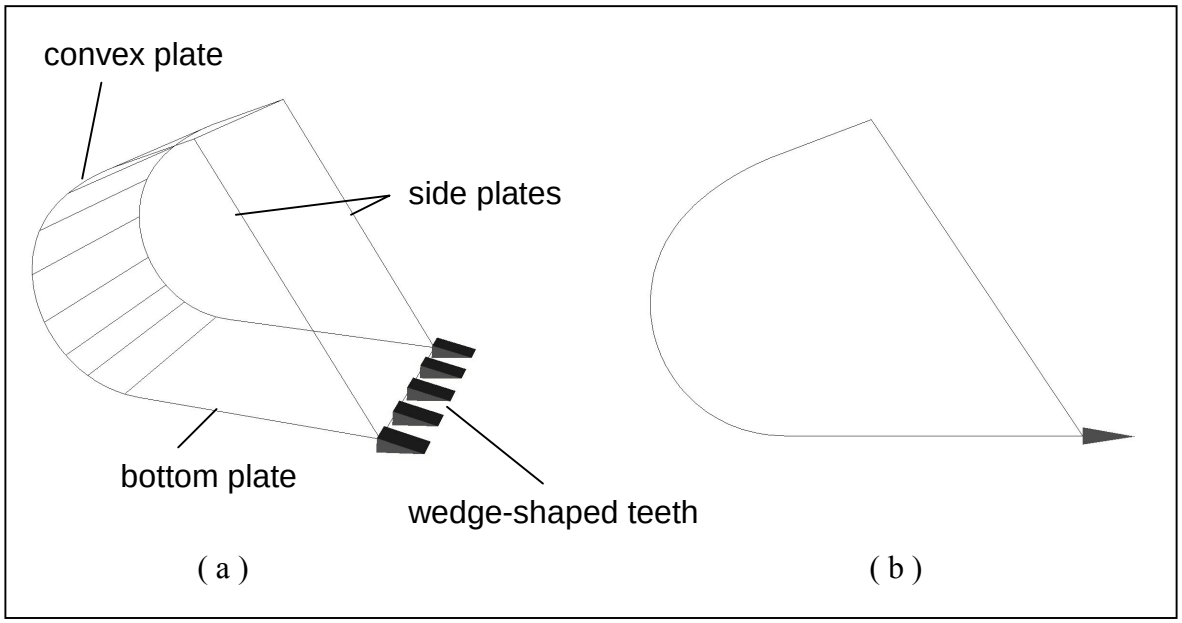

Figure 5.2 Typical Bucket: (a) Perspective View and (b) Side View

Firstly, the bucket teeth function as soil breaking parts by penetrating the media. The shape of the tooth usually resembles a wedge form because its tapered cross-section facilitates a penetration process by providing proper pressures continuously to push itself into the soil media. Therefore, the shape approximation must preserve this characteristic to be a reasonable replacement. In this regard, the wedge-shaped bucket is well approximated by a cone-shaped tooth as shown in Figure 5.3. The dimension of this idealized bucket tooth should be close to that of the original bucket.

Secondly, the bottom plate is mainly used to provide forces by which soil body contacting above it can be separated and displaced to a failure state (Note that this bottom plate is also involved in part in a penetration process by being a source of friction force with soil). Therefore, this functional characteristic is easily fulfilled by replacing the plate with a rectangular shaped plate as shown in Figure 5.3. This plate is referred to as a *separation plate* due to its functional role in breaking soil. Even though the existence of

the side plates is not reflected in the simplification above, the effect of the side plates on the separation resistance is included in the model development in the later section.

Lastly, the convex plate and the two side plates mainly contribute to the reason that ripped soil gets filled and packed inside a bucket and eventually forms some kind of imaginary plane by which the soil in front of it experiences additional separation failure as described in Section 2.5. Therefore, another rectangular plate, forming a normal angle with the separation plate, is the idealized part used to account for this lapsed separation mechanism as shown in Figure 5.3. This plate is termed the secondary separation plate.

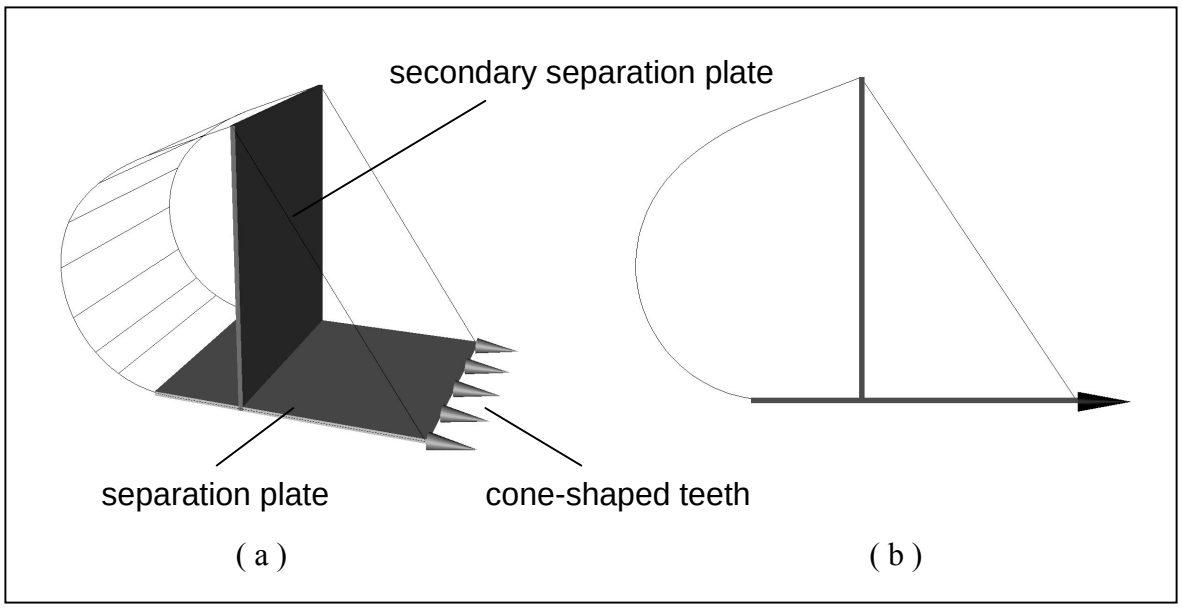

Figure 5.3 Bucket Overlapped with Idealized Parts:
(a) Perspective View and (b) Side View

As a result of this transformation process, the typical bucket shape presented in Figure 5.2 has been idealized to the shape depicted in Figure 5.4. These idealized bucket parts are assumed be equivalent to their original counter parts in terms of generating penetration, separation and secondary separation resisting forces given that the models proposed in later sections are based on this idealized bucket shape.

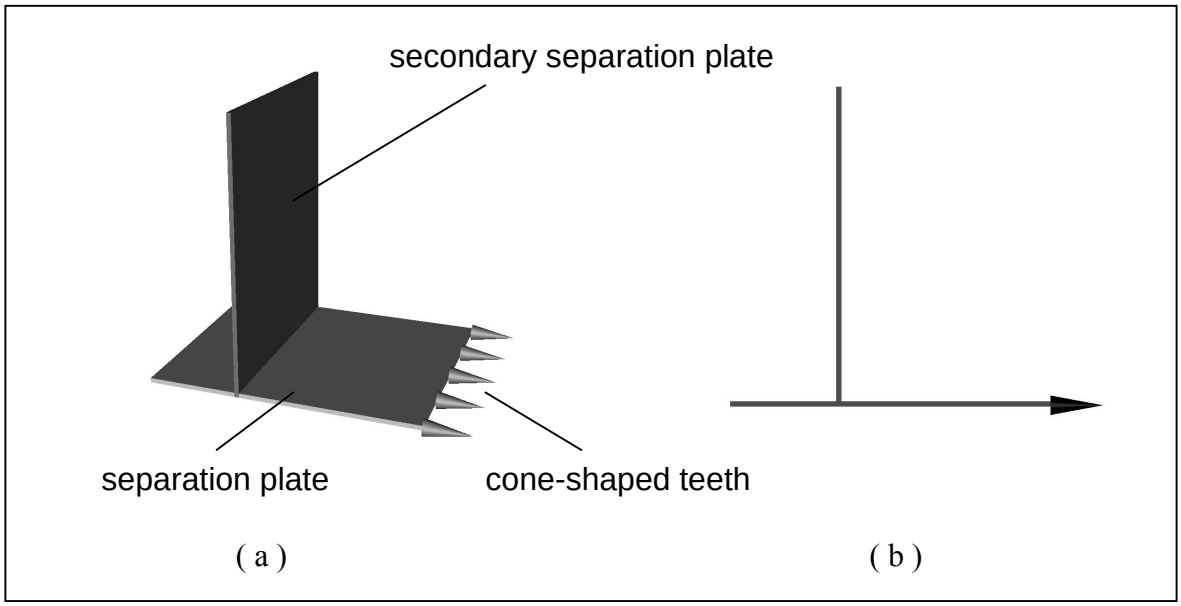

Figure 5.4 Idealized Bucket: (a) Perspective View and (b) Side View

5.3 Generalized Separation Model

It has been discussed that 3-D analytical resistance models are better suited to explain soil resistance induced by separation-mechanism-based excavating tool. This is because the 3-D resistance models predict soil resistance reasonably well by analytically representing forces involved in the soil-tool interaction with 3-dimensional soil failure geometries whereas 2-D analytical models and the empirical models are unable to do this. Among these 3-D resistance models, the Perumpral's model (Perumpral, Grisso and Desai 1983) is selected in this research as the basic model, from which the excavator bucket separation model is developed. This 3-D analytical model is appropriate in this separation model generalization for the following reasons:

1) it allows a relatively simple soil failure shape without relying on experimental results; and
2) its proposed failure shape is close to the one created by an excavator bucket as shown in the right side of Figure 5.5, which also shows the failure geometry of McKyes' model (McKyes 1985) for the comparison.

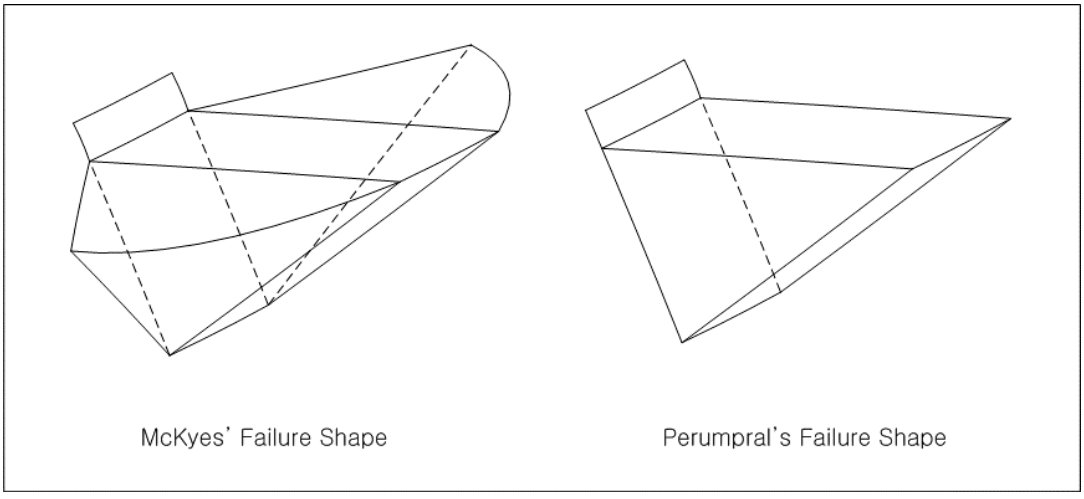

Figure 5.5 Proposed Failure Shapes of Godwin's model and Perumpral's model

However, Perumpral's model needs to be expanded such that it can predict separation soil resistance in an inclined terrain, which is an usual terrain condition in excavator digging cases. The model also needs to incorporate excavator bucket shape, specifically the two side plates since the Perumpral's model is based on a rectangular plate without side plates. To this end, a generalized separation model is developed using the same analytical method used in the Perumpral's model.

5.3.1 Idealized Soil Failure Wedge

The generalized separation model starts from a 3-dimensional idealized soil failure wedge (Figure 5.6) consisting of an idealized bucket separation plate in contact with soil (' abed '), a terrain surface (' acfd '), two triangular side rupture surfaces (' abc ' and ' def ') and a rectangular failure surface (' bcfe '). This shape of the failure wedge is similar to that used in Perumpral's model except for the inclusion of an inclined terrain surface. The other difference is that Perumpral's model implicitly assumes crescentic soil failure on tool sides as shown in the left side of Figure 5.5 and replaces it with two triangular failure surfaces: however, in this generalized separation model for an excavator bucket, the two side failure planes (' abc ' and ' def ') themselves are a legitimate approximation to the actual soil rupture created by a bucket with two side plates.

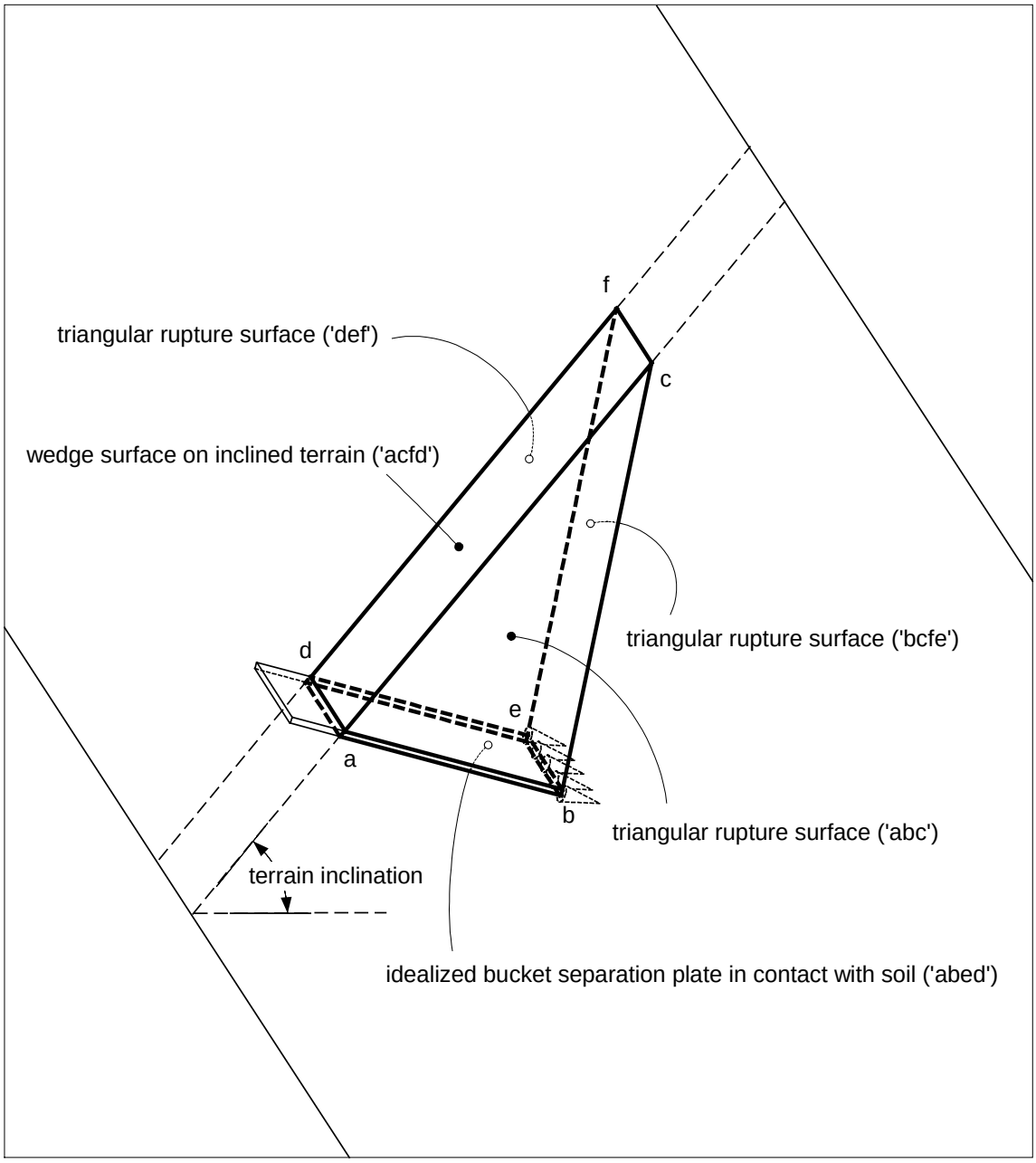

Figure 5.6 3-Dimensional Geometric Boundaries of Idealized Separation Failure Wedge

5.3.2 Identification of Forces Related to Separation Failure

Based upon the soil failure wedge, all the forces acting on appropriate surfaces are identified as shown in Figure 5.7. These forces eventually contribute to a separation resisting force (***Rs***). The description of each force component is as follows.

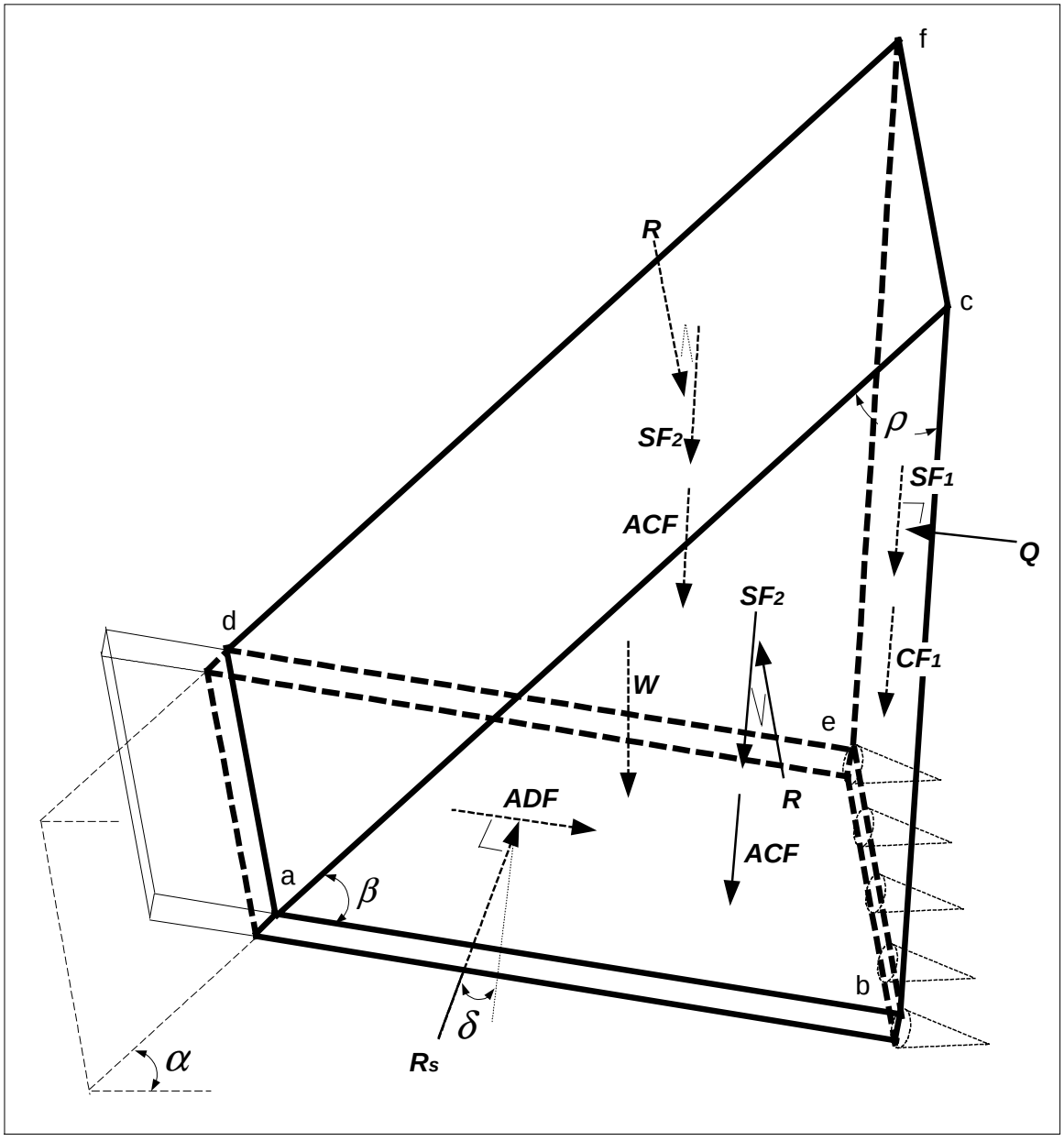

Figure 5.7 Separation Resistance Force Breakdown

Where,

- ***Rs*** : separation resisting force consisting of a parallel friction and a normal force to the surface 'abed'
- ***ADF*** : adhesional force acting on the surface 'abed' due to the adhesion between the plate and the soil
- ***W*** : gravitational force of the soil wedge
- ***Q*** : normal force acting on the rectangular failure surface 'bcfe'
- SF_1 : frictional force acting on the rectangular failure surface 'bcfe' due to the friction between soil particles on the interface $= Q \cdot \tan\Phi$
- CF_1 : cohesional force acting on the rectangular failure surface 'bcfe' due to the cohesion between soil particles
- ***R*** : equal and opposite normal force acting on the triangular side failure surface 'abc' or 'def '
- SF_2 : frictional force acting on the triangular side failure surface 'abc' or 'def ' due to the friction between soil particles on the interface
- ***ACF*** : adhesional-cohesional force acting on the triangular side failure surface 'abc' or 'def ' due to the adhesion between the side plates and the soil and the cohesion between soil particles

- α : angle between the inclined terrain surface and the horizontal plane
- β : angle between the separation plate and the inclined terrain surface
- ρ : angle between the soil failure plane and the inclined terrain surface (soil failure angle)
- δ : soil-metal friction angle
- Φ : soil internal friction angle

In order to include the contribution of the bucket side plates to the resistance in the separation process, the adhesional-cohesional forces (***ACF***) on the triangular failure surfaces have been included. This is different from Perumpral's model, which

includes only the cohesional force. With this force included, the idealized shape of a bucket doesn't need to have the side plates as shown in Figure 5.7.

*5.3.3 Derivation of Separation Resistance (**Rs**)*

The separation resisting force (***Rs***) can be determined by solving the equilibrium with the conditions specified in Figure 5.7. Since the forces in y direction are opposite in their directions and equal in their magnitudes, the 2-dimensional representation in the x-z plane (Figure 5.8) is enough to calculate the resisting force (***Rs***).

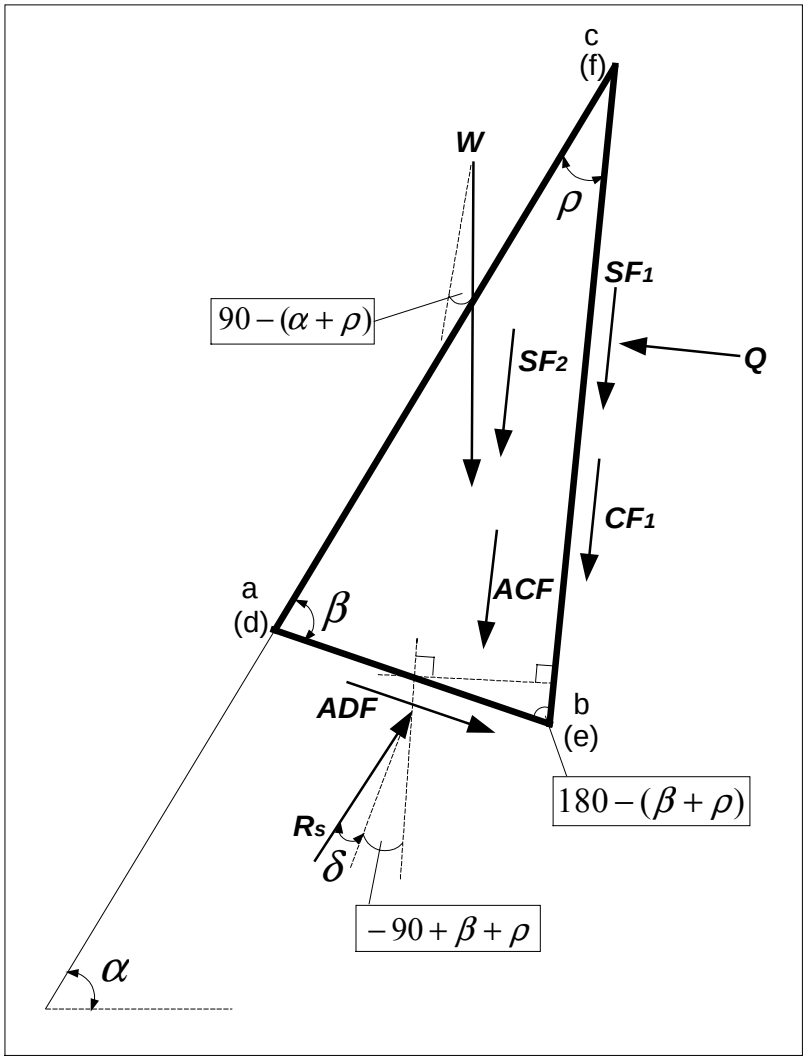

Figure 5.8 Separation Resistance Force Breakdown in 2-D

ΣF *parallel to the failure plane = 0:*

➔ $-Rs \cdot \cos(-90+\beta+\rho+\delta) + ADF \cdot \cos[180-(\beta+\rho)] + CF_1 + SF_1 + 2 \cdot ACF + 2 \cdot SF_2 + W \cdot \cos[90-(\alpha+\rho)] = 0$

➔ $-Rs \cdot \sin(\beta+\rho+\delta) - ADF \cdot \cos(\beta+\rho) + CF_1 + Q \cdot \tan\Phi + 2 \cdot ACF + 2 \cdot SF_2 + W \cdot \sin(\alpha+\rho) = 0$ (5-1)

ΣF *normal to the failure plane = 0:*

➔ $W \cdot \sin[90-(\alpha+\rho)] + ADF \cdot \sin[180-(\beta+\rho)] + Rs \cdot \sin(-90+\beta+\rho+\delta) - Q = 0$

➔ $Q = W \cdot \cos(\alpha+\rho) + ADF \cdot \sin(\beta+\rho) - Rs \cdot \cos(\beta+\rho+\delta)$ (5-2)

By combining (5-2) into (5-1), the resistance force (**Rs**) is derived as follows.

➔ $-Rs \cdot \sin(\beta+\rho+\delta) - ADF \cdot \cos(\beta+\rho) + CF_1 + [W \cdot \cos(\alpha+\rho) + ADF \cdot \sin(\beta+\rho) - Rs \cdot \cos(\beta+\rho+\delta)] \cdot \tan\Phi + 2 \cdot ACF + 2 \cdot SF_2 + W \cdot \sin(\alpha+\rho) = 0$

➔ $Rs = \{-ADF \cdot [\cos(\beta+\rho) - \sin(\beta+\rho) \cdot \tan\Phi] + W \cdot [\sin(\alpha+\rho) + \cos(\alpha+\rho) \cdot \tan\Phi] + CF_1 + 2 \cdot ACF + 2 \cdot SF_2 \} / \{\sin(\beta+\rho+\delta) + \cos(\beta+\rho+\delta) \cdot \tan\Phi\}$

➔ $Rs = \{-ADF \cdot [\cos(\beta+\rho) \cdot \cos\Phi - \sin(\beta+\rho) \cdot \sin\Phi] + W \cdot [\sin(\alpha+\rho) \cdot \cos\Phi + \cos(\alpha+\rho) \cdot \sin\Phi] + CF_1 \cdot \cos\Phi + 2 \cdot ACF \cdot \cos\Phi + 2 \cdot SF_2 \cdot \cos\Phi \} / \{\sin(\beta+\rho+\delta) \cdot \cos\Phi + \cos(\beta+\rho+\delta) \cdot \sin\Phi\}$

$$\therefore Rs = \frac{-ADF \cdot \cos(\beta+\rho+\phi) + W \cdot \sin(\alpha+\rho+\phi) + CF_1 \cdot \cos\phi + 2 \cdot ACF \cdot \cos\phi + 2 \cdot SF_2 \cdot \cos\phi}{\sin(\beta+\rho+\delta+\phi)} \quad (5\text{-}3)$$

As expected, the derived separation resistance formula (5-3) is different when compared to the Perumpral's original formula only by the inclusion of α (terrain inclination) in the weight (***W***)-term and the adhesional-cohesional force (***ACF***). The calculation of each force component is described in the following based on the Figure 5.9.

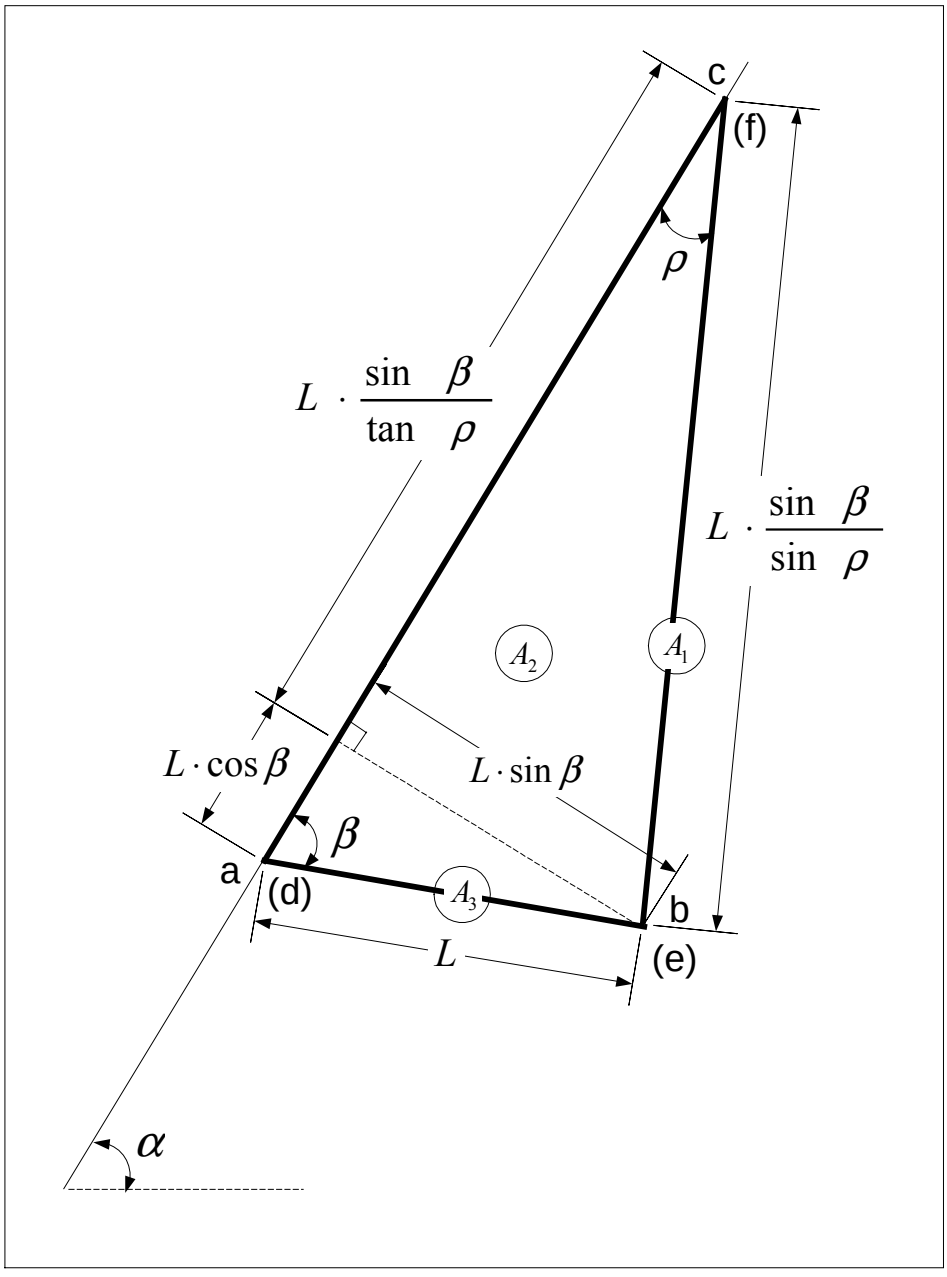

Figure 5.9 Soil Failure Wedge Dimensions for Calculation of Force Components

- $ADF = c_a \cdot A_3 = c_a \cdot B \cdot L$ (5-4)

  c_a: soil adhesion
  A_3: area of bucket separation plate in contact with soil ('abed')
  B: separation plate width
  L: length of separation plate in contact with soil

- $W = \gamma \cdot B \cdot A_2 = \gamma \cdot B \cdot [0.5 \cdot (L \cdot \sin\beta) \cdot (L \cdot \cos\beta + L \cdot \sin\beta / \tan\rho)]$
  $= 0.5 \cdot \gamma \cdot B \cdot L^2 \cdot \sin\beta \cdot (\cos\beta + \sin\beta / \tan\rho)$ (5-5)

  γ: soil unit weight
  A_2: area of triangular rupture surface ('abc' or 'def')

- $CF_1 = c \cdot A_1 = c \cdot B \cdot L \cdot \sin\beta / \sin\rho$ (5-6)

  c: soil cohesion
  A_1: area of rectangular failure surface ('bcfe')

- $ACF = c^* \cdot A_2 = c^* \cdot [0.5 \cdot (L \cdot \sin\beta) \cdot (L \cdot \cos\beta + L \cdot \sin\beta / \tan\rho)]$
  $= 0.5 \cdot c^* \cdot L^2 \cdot \sin\beta \cdot (\cos\beta + \sin\beta / \tan\rho)$ (5-7)

  c^*: soil adhesion-cohesion

- $SF_2 = K_0 \cdot \gamma \cdot z \cdot \tan\Phi^* \cdot A_2$
  $= 0.5 \cdot K_0 \cdot \gamma \cdot z \cdot \tan\Phi^* \cdot L^2 \cdot \sin\beta \cdot (\cos\beta + \sin\beta / \tan\rho)$ (5-8)

  K_0 : coefficient of lateral earth pressure at rest
  z: depth from the wedge top(point 'c' or 'f') to the wedge centroid
  Φ^*: combined friction angle of δ(soil-metal friction angle) and
  Φ(soil internal friction angle)

In (5-7) and (5-8), the soil adhesion-cohesion (c^*) and the combined friction angle (Φ^*) are determined by dividing the area of the side plate by area of the wedge triangular rupture surface. In other words, as demonstrated in Figure 5.10, the triangle area 'abx' is the interface between the side plate and the soil and the area 'bcx' is the interface

between the soil inside the wedge and the soil outside the wedge, on which ***ACF*** and ***SF₂*** are acting. Therefore, for the area 'abx', the responsible soil properties for ***ACF*** and ***SF₂*** are the soil adhesion (a_d) and the tool-soil friction angle (δ), respectively. By the same token, for the area 'bcx', the responsible soil properties are the soil cohesion (c) and the internal soil friction angle (Φ) for ***ACF*** and ***SF₂***, respectively. Therefore, the soil adhesion-cohesion (c^*) and the combined friction angle (Φ^*) can be determined as follows.

$$c^* = \frac{c_a \cdot Area_{abx} + c \cdot Area_{bcx}}{Area_{abc}} \tag{5-9}$$

$$\phi^* = \frac{\delta \cdot Area_{abx} + \phi \cdot Area_{bcx}}{Area_{abc}} \tag{5-10}$$

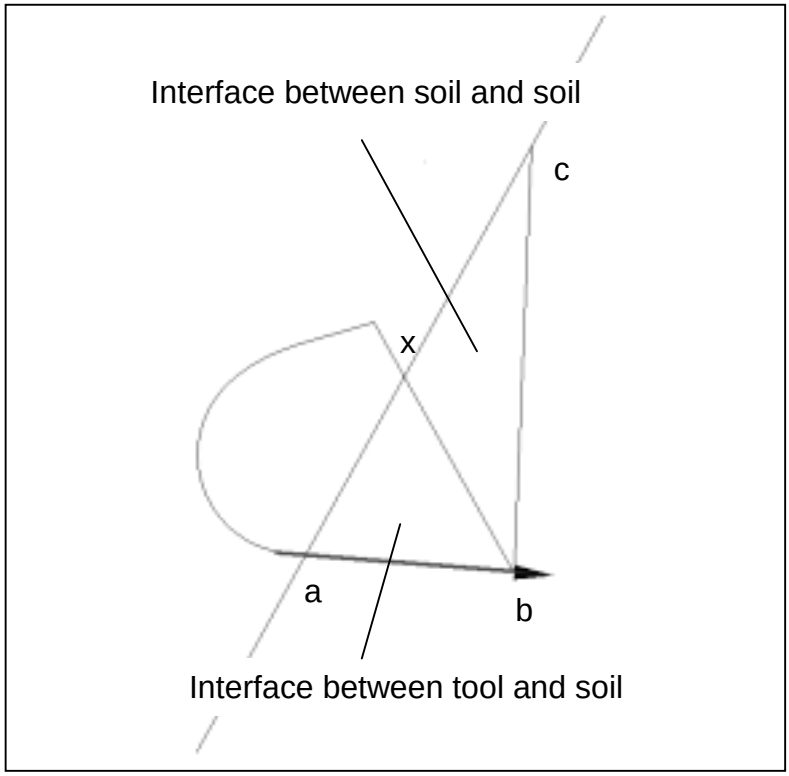

Figure 5.10 Tool-soil vs. soil-soil interfaces on the side-wedge rupture surface

The depth from the wedge top to the wedge centroid (z) in (8) is calculated as follows with the aid of Figure 5.11.

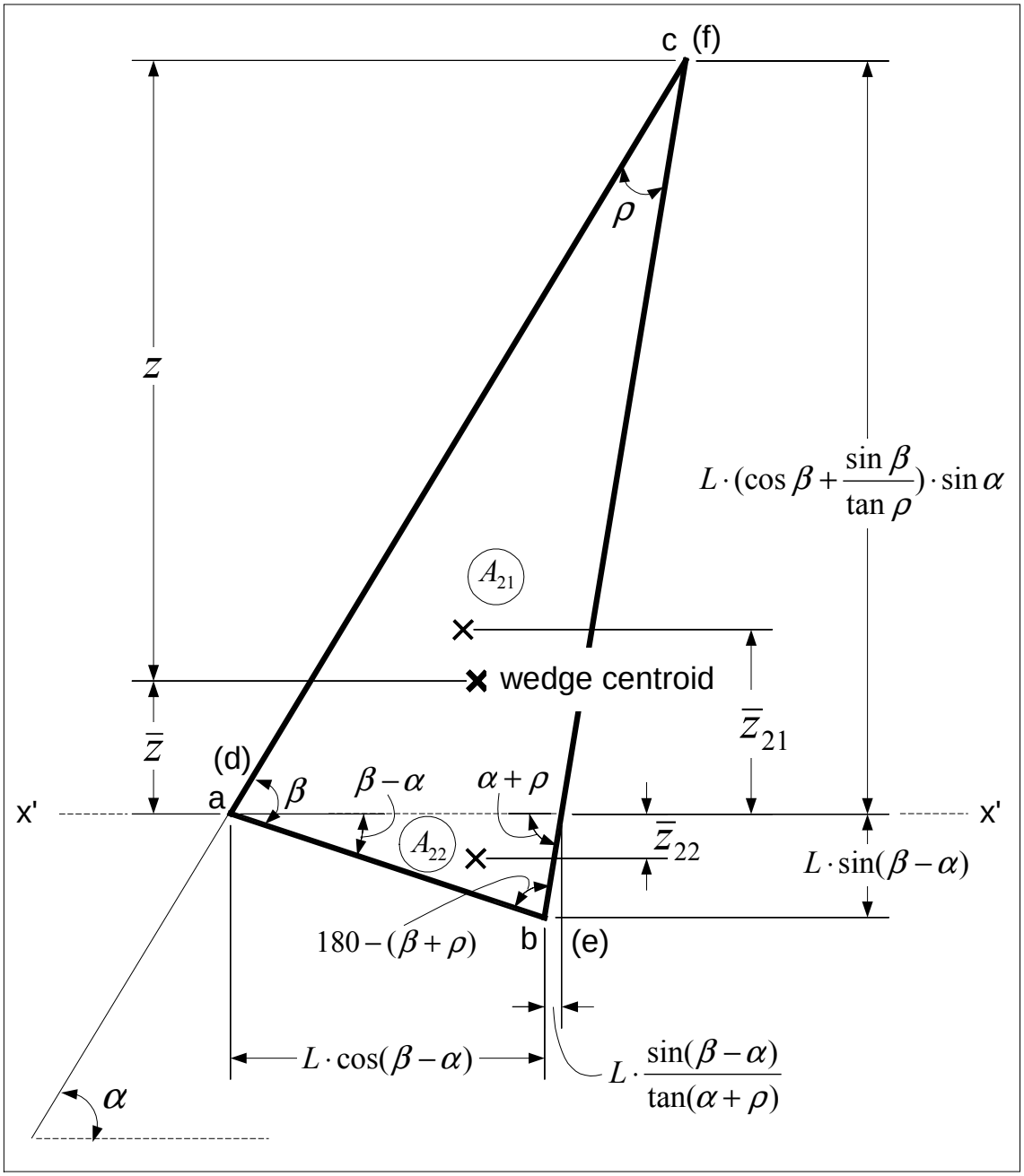

Figure 5.11 Dimensions for Wedge Centroid Calculation

$\begin{cases} x'\text{-}x' \text{: arbitrary axis for moment calculation} \\ A_{21} \text{: area of the upper triangle cut by the axis } x'\text{-}x' \\ A_{22} \text{: area of the lower triangle cut by the axis } x'\text{-}x' \\ \bar{z} \text{ : distance from the wedge centroid to the axis } x'\text{-}x' \\ \bar{z}_{21} \text{: distance from the centroid of } A_{21} \text{ to the axis } x'\text{-}x' \\ \bar{z}_{22} \text{: distance from the centroid of } A_{22} \text{ to the axis } x'\text{-}x' \end{cases}$

The first moments of areas A_{21}, A_{21}, $(A_{21}+A_{21})$ with respect to the axis x'-x' are first calculated to determine the centroid of the wedge.

$$(A_{21}+A_{22})\cdot\bar{z} = A_{21}\cdot z_{21} + A_{22}\cdot z_{22}$$

$$\rightarrow \; 0.5\cdot L^2\cdot\sin\beta\cdot(\cos\beta+\frac{\sin\beta}{\tan\rho})\cdot\bar{z} =$$

$$0.5\cdot L\cdot[\cos(\beta-\alpha)+\frac{\sin(\beta-\alpha)}{\tan(a+\rho)}]\cdot L\cdot(\cos\beta+\frac{\sin\beta}{\tan\rho})\cdot\sin\alpha\cdot[\frac{L}{3}\cdot(\cos\beta+\frac{\sin\beta}{\tan\rho})\cdot\sin\alpha]$$

$$+0.5\cdot L\cdot[\cos(\beta-\alpha)+\frac{\sin(\beta-\alpha)}{\tan(a+\rho)}]\cdot L\cdot\sin(\beta-\alpha)\cdot[-\frac{L\cdot\sin(\beta-\alpha)}{3}]$$

$$\rightarrow \; \bar{z} = \frac{L}{3}\cdot\frac{[\cos(\beta-\alpha)+\frac{\sin(\beta-\alpha)}{\tan(\alpha+\rho)}]\cdot[\sin^2\alpha\cdot(\cos\beta+\frac{\sin\beta}{\tan\rho})^2-\sin^2(\beta-\alpha)]}{\sin\beta\cdot(\cos\beta+\frac{\sin\beta}{\tan\rho})}$$

$$\therefore z = L\cdot(\cos\beta+\frac{\sin\beta}{\tan\rho})\cdot\sin\alpha$$

$$-\frac{L}{3}\cdot\frac{[\cos(\beta-\alpha)+\frac{\sin(\beta-\alpha)}{\tan(\alpha+\rho)}]\cdot[\sin^2\alpha\cdot(\cos\beta+\frac{\sin\beta}{\tan\rho})^2-\sin^2(\beta-\alpha)]}{\sin\beta\cdot(\cos\beta+\frac{\sin\beta}{\tan\rho})} \qquad (5\text{-}11)$$

By assembling the formulas (5-3) through (5-11), the separation resisting force ***(Rs)*** is represented as a function of the variables shown in below.

$$R_s = f(\rho, \alpha, \beta, \varphi, \delta, c, c_a, \gamma, K_0, B, L) \tag{5-12}$$

Where,

- ρ : angle between the soil failure plane and the inclined terrain surface (soil failure angle)
- α : angle between the inclined terrain surface and the horizontal plane
- β : angle between the separation plate and the inclined terrain surface
- Φ : soil internal friction angle
- δ : soil-metal friction angle
- c : soil cohesion
- c_a : soil adhesion
- K_0 : coefficient of lateral earth pressure at rest
- B : separation plate width
- L : length of separation plate in contact with soil

The separation resistance can be predicted if the failure angle (ρ) of the soil wedge is known. As in the case of Perumpral's model, the soil failure angle (ρ) can be determined by adopting passive earth pressure theory (Terzaghi 1959). This states that passive failure occurs when the resistance offered by the soil wedge is minimum. Therefore, by finding the minimum value of ***Rs***, the separation resisting force can be determined.

5.4 Penetration Model

As described in the previous section (Section 2.4.2), a penetration failure is better explained by the cavity expansion theory than the bearing capacity theory because of its flexibility and consistency as well as its ability to include appropriate soil behavior and penetration process. Therefore, in this section, the cavity expansion theory is used as the main device for determining the resistance required to penetrate soil media.

5.4.1 Identification of Forces Contributing to Penetration Resistance (R_p)

When a bucket engages in the penetration process, it involves bucket teeth as well as a separation plate as shown in Figure 5.12.

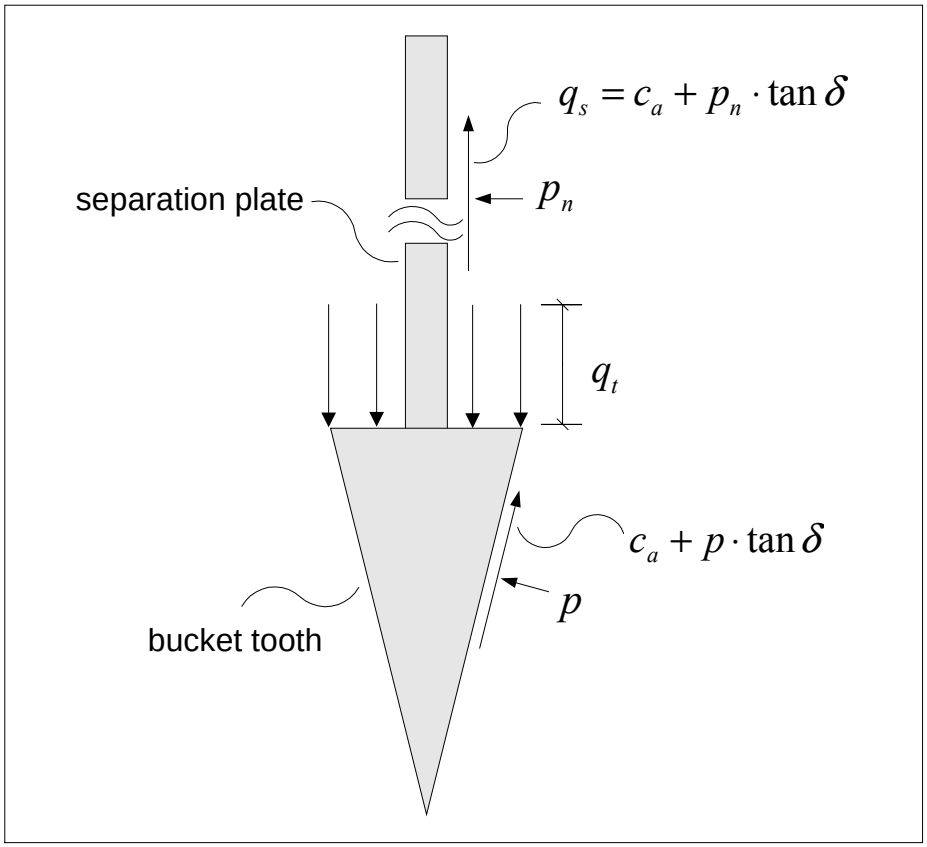

Figure 5.12 Breakdown of Total Penetration Resisting Force (R_P)

The total penetration resistance (***R**p*), therefore, consists of the resistance from the separation plate (***R**ps*) and the resistance from the teeth (***R**pt*).

$$R_p = R_{ps} + R_{pt} \tag{5-13}$$

As shown in the Figure 5.12, the resistance ***R**ps* is comprised of adhesional (c_a) and frictional (δ) force components acting on the center of the surface of the separation plate. The normal soil pressure (p_n) on the separation plate is determined from the angle of the separation plate in soil. When the separation plate is horizontal, p_n is calculated to be γz (z: depth from the surface to the centroid of the separation plate) and when the plate is vertical in the soil, p_n is $K_0 \cdot \gamma z$ (K_0: coefficient of lateral earth pressure at rest). For other cases where the separation plate is inclined, p_n can be determined by constructing a Mohr's circle. As a result, the penetration resistance from the separation plate (***R**ps*) is calculated as follows.

$$R_{ps} = q_s \cdot A_s = (c_a + p_n \cdot \tan\delta) \cdot A_s \tag{5-14}$$

(A_s: *area of the separation plate*)

The resistance to penetration by the teeth (***R**pt*), the main quantitative target in the penetration resistance, can be calculated from a tooth penetration pressure (q_t). The tooth penetration pressure (q_t) is the equivalent of the adhesion (c_a) and friction (δ) components on the surface of the tooth as well as the cavity expansion pressure (p) itself through which the initially small cavity grows to the size enough for the tooth to be accommodated. Differently put, the calculation of the cavity-expansion-based tooth penetration pressure (q_t) is divided into two stages (Farrell and Greacen 1966; Ladanyi and Johnston 1974; Yasufuku and Hyde 1995; Yu and Mitchell 1998). The first stage is where the cavity expansion pressure (p) has increased the incipient small hole (cavity) to the required (desired) cavity volume (with radius a). Then the second stage is where the cavity expansion pressure (p) is linked to the tooth penetration pressure (q_t).

For determining the cavity expansion pressure (p) of the first stage, any cavity expansion model can be used. In this research, Yu's cavity expansion model (Yu and Houlsby 1991) is used because it does not depend on soil experiments for the deformation information, and it provides the explicit solution for the cavity pressure. The procedure to calculate the cavity pressure p is summarized in the Appendix A. As previously pointed out in the Section 2.4.2.B, however, the cavity expansion theory has some problems in its applicability in a bucket-tooth penetration process. These issues are discussed in the next section.

Once the cavity expansion pressure (p) is obtained, the conversion (of the second stage) is made by assuming that "the lateral surface of the cone is acted upon by a uniformly distributed soil pressure whose normal component is equal to the cavity expansion pressure *(p)* (Farrell and Greacen 1966; Ladanyi and Johnston 1974)" as shown in Figure 5.13. The relationship is derived as follows.

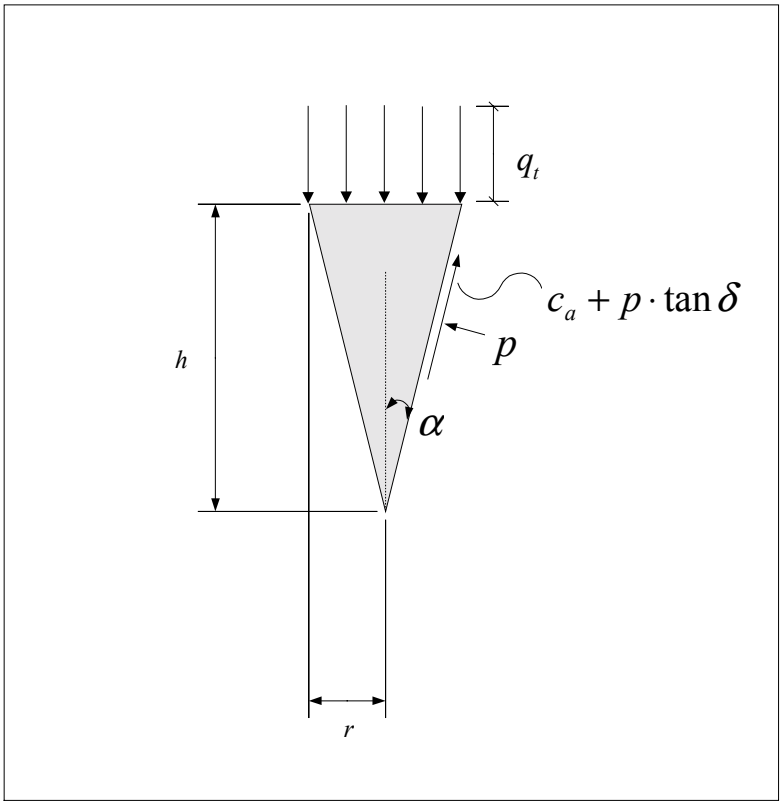

Figure 5.13 Conversion from a Cavity Pressure *(p)* to a Tooth Penetration Pressure *(q_t)*

$\Sigma F_{vertical} = 0$:

➔ $$\pi \cdot r^2 \cdot q_t = \{(c_a + p \cdot \tan\delta) \cdot [\pi \cdot r \cdot (h \cdot \sec\alpha)]\} \cdot \cos\alpha + p \cdot [\pi \cdot r \cdot (h \cdot \sec\alpha)] \cdot \sin\alpha$$

➔ $q_t = p + (c_a + p \cdot \tan\delta) \cdot \cot\alpha$ (α : tip semi angle)

As a result, the penetration resistance from the tooth (***R_{pt}***) is calculated as follows.

$$R_{pt} = n \cdot q_t \cdot A_t = n \cdot [p + (c_a + p \cdot \tan\delta) \cdot \cot\alpha] \cdot A_t \quad (5\text{-}15)$$

(A_t*: area of the cone top* and *n: number of teeth*)

5.4.2 Assumptions on Cavity Expansion Theory for Bucket Tooth Penetration

The cavity expansion theory has some problems when it is used in bucket tooth induced penetration cases as described in the previous section (Section 2.4.2.B). In the following, these problems are addressed by making appropriate assumptions.

- ***Matching shape of bucket tooth with cavity***

The cavity expansion theory assumes an ideally growing cavity in soil media either in a spherical form or in a cylindrical form. This inherently means that the cavity expansion pressure to form such a cavity is provided by a device whose shape is a sphere or cylinder. Therefore the assumption creates the inevitable discrepancy between the shape of the actual penetration tool (cone-shaped tooth) and the shape of an ideal cavity form. Consequently, the applicability of the cavity expansion theory very much relies on how well the bucket tooth can be matched with the cavity shape. Therefore, there should be a consideration to match this conical shape of the tooth to the shape of a cavity. In this regard, a few approximations are proposed in Figure 5.14 with their assumptions and pertinence to the conical-shape tooth penetration. Note that the diagrams present a 2-dimensional view of the three dimensional case, with circles representing spheres and triangles representing cones.

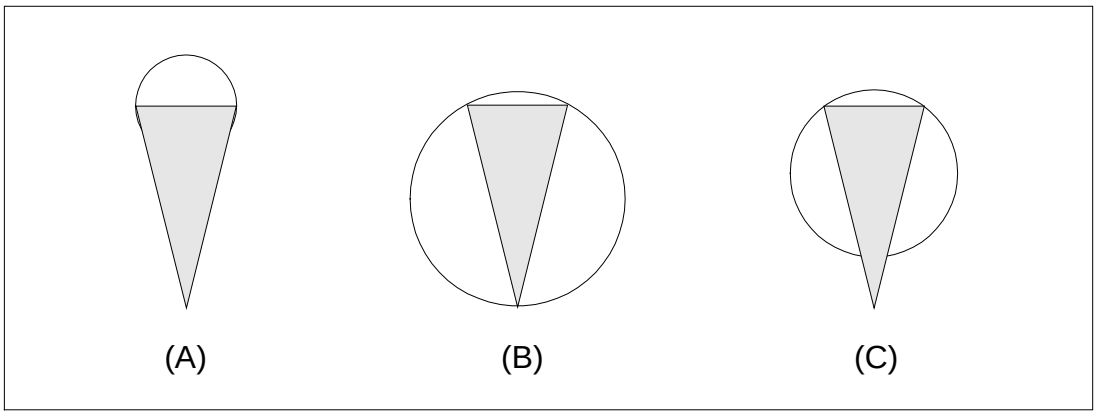

Figure 5.14 Various Matches for Cone Tip and Cavity

In the diagram (A), the cavity has grown just enough to fit with the largest cross sectional area of the tooth (top section). However, the cavity is not big enough as far as the tooth height is concerned. In other words, the most volume of the tooth is excluded from the cavity. Therefore it is likely that the cavity expansion pressure is underestimated. The diagram (B) shows the opposite situation of (A), where the cavity gets big enough to accommodate the whole conical tooth. It is, however, too large to be a feasible substitution for the tooth. This situation implies that the cavity expansion pressure is overestimated. The diagram (C) represents a case where most part of the conical body of the tooth is included in the cavity with the largest cross-sectional area of the tooth (tooth top) embedded in the sphere. Therefore it is a better choice than case (A) and case (B). Note that the size of the cavity matched to the bucket tooth is directly used for determining the cavity expansion pressure (p).

- ***Providing initial cavity (a_0)***

The spherical cavity expansion theory explains that a penetration process starts from an initial spherical cavity with a radius a_0 and initial pressure p_0, which continuously grows into a bigger cavity. However, the theory lacks an explanation of how to provide these initial conditions. Therefore, another assumption should be made in terms of providing initial cavity for the continuously penetrating bucket tooth. To this end, the portion of the tooth outside the cavity identified in the (C) in the Figure 5.14 is assumed to function as an initial cavity. Once the tooth penetrates into the soil, the forefront conical part is then providing the initial space from which the next cavity can be developed. As a result, the tooth is able to put itself into the expanded cavity and this process keeps repeating. This process can be thought of as a discretely continuous penetration process that resembles a true continuous penetration process. Detailed description is presented in the following section.

5.4.3 Penetration Process

The penetration process of a bucket tooth is assumed to occur in discrete steps as shown in Figure 5.15 and described in the following paragraph.

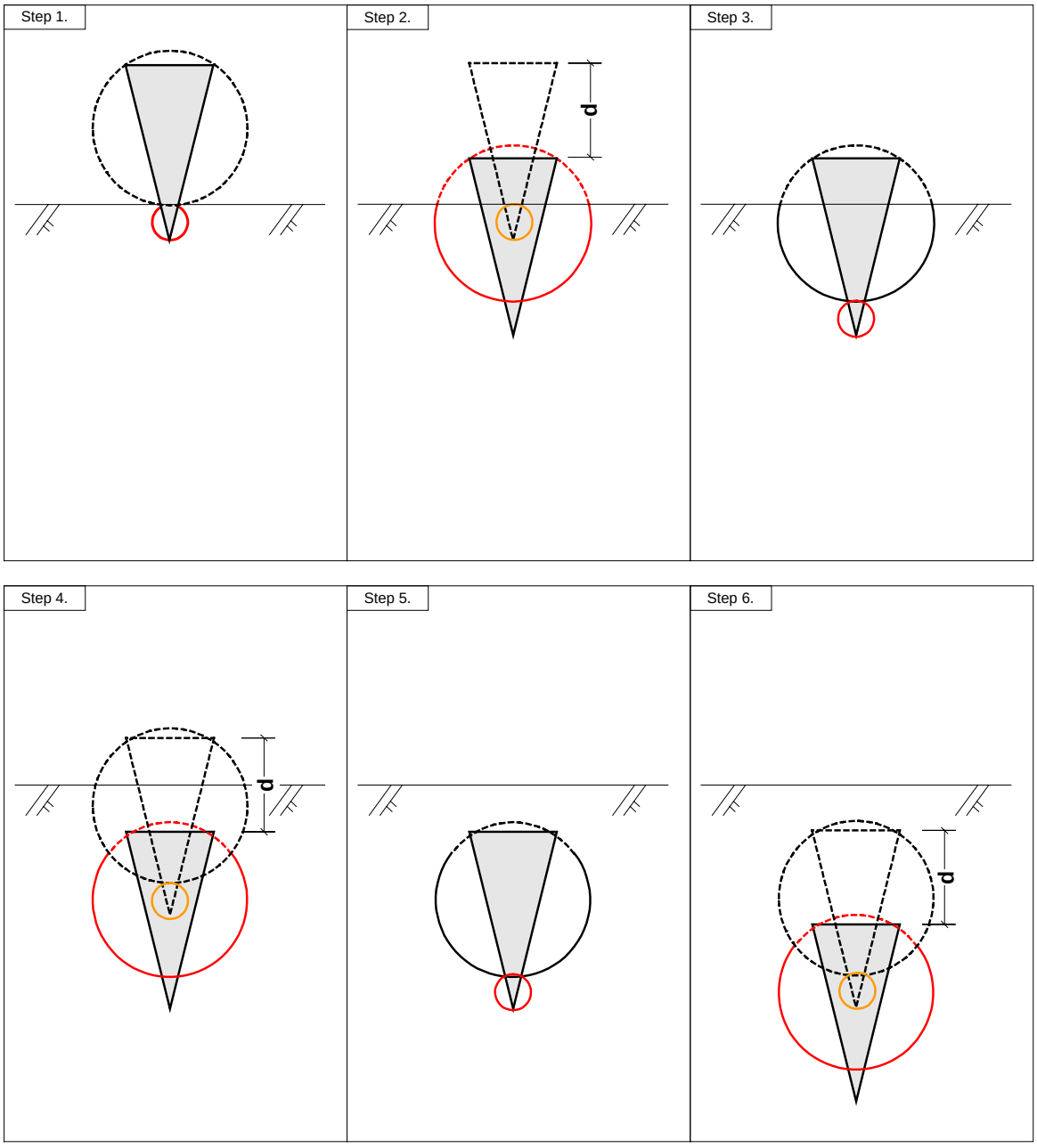

Figure 5.15 Bucket Tooth Penetration Process

In the step 1, the bucket tooth is about to penetrate into the soil. The initial cavity marked by a red circle is the space occupied by the tip of the tooth. The initial cavity pressure ($\boldsymbol{p_0}$) is assumed to be the earth pressure at rest with the depth corresponding to the radius a_0 of the initial cavity. As the tooth is being pushed downward (step 2), this initial cavity starts to grow and expand until it gets to a required size marked by a red circle. At this step, the cone has advanced as much as d. The cone tip outside the circle (step 3) now functions as another initial cavity $\boldsymbol{(a_0)}$ for the next stage. This small cavity grows to be fully expanded for the tooth to be accommodated as shown in the step 4, in which the tooth has advanced further to the distance d. At this point, the separation plate above the tooth starts to go down to earth along with the tooth, which experiences just frictional and adhesional resistance as explained earlier. In the steps 5, 6, and …, the same cavity expansion and advancement of the cavity will be repeating until the bucket gets to the desired depth.

Note that although the bottom edge of the rectangular plate between the teeth is contacting the soil directly, its penetration involving the expansion phenomenon need not be considered. That is because the cavities developed by each tooth forms the enough plastic region around them so that soil bondage between the teeth can be assumed to be broken.

5.5 Excavator Digging Modes

Even though the separation model and the penetration model for an idealized excavator bucket are developed, they do not represent all the possible digging actions encountered in excavator digging because three mechanisms (separation, secondary separation and penetration) constantly put different contributions to the generation of soil resistance in the digging process. By virtue of the motional versatility of an excavator machine, the different mechanisms are mixed at any stage of digging process to generate any arbitrary digging action. To complement such a deficiency of those models, digging action groups or digging modes are proposed in this section. The purpose of digging modes is to provide means for any particular digging action to be classified into a certain digging situation (digging mode) so that its underlying digging mechanism or mechanisms are identified and, therefore, resistance for each mechanism is calculated using the models developed in the previous sections. To serve this purpose, the digging modes represent abstracted representation for all digging actions, whose underlying mechanisms correspond to a separation, a penetration, a secondary separation or combination of some or all of the mechanisms. In this section, various digging modes are explained. The conditions that constitute each digging mode are detailed with the aid of some exemplary digging actions. All digging modes are presented in Figure 5.16 and the description of each digging mode follows.

Note that these digging modes are the classification of the findings through small-scale excavation experiments, and motion analyses of excavation video clips and pictures. Figure 5.17, for example, shows a series of pictures taken from a small-scale excavation experiment, in which two digging modes are observed. In picture 1, the bucket is introduced into the soil horizontally as shown in the upper diagram. At this stage, the bucket only experiences the penetration resistance from the soil (digging mode II: penetration). In picture 2, the bucket is still in the digging mode II. However, as the bucket proceeds further in picture 3, it experiences additional resistance (secondary separation) on the top of the penetration resistance (digging mode IV: penetration + secondary separation). The last pictures (4 and 5) show the failure shape of the soil in the digging IV. Further explanation on the secondary separation is included in Section 2.6.

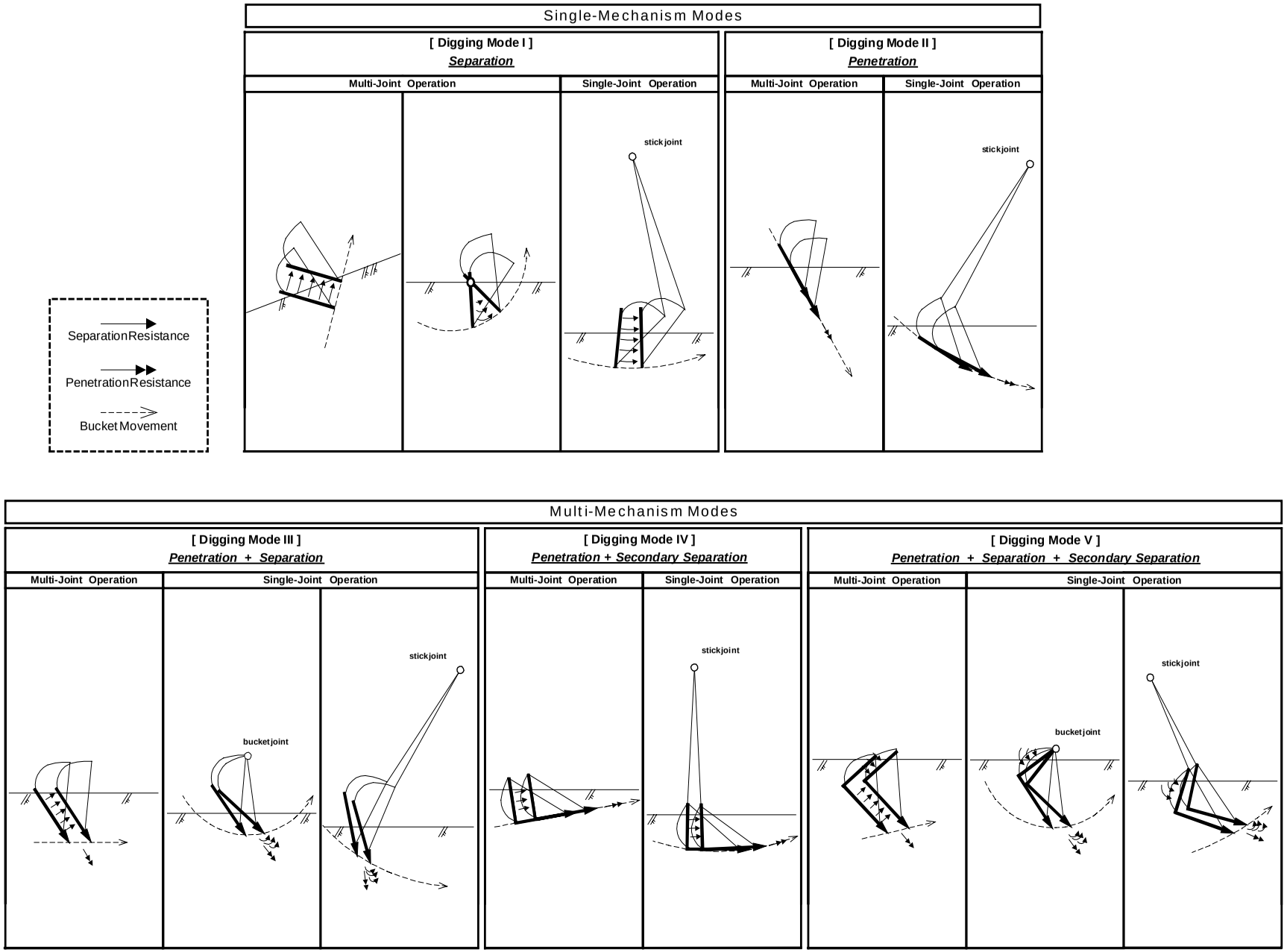

Figure 5.16 Excavator Digging Modes

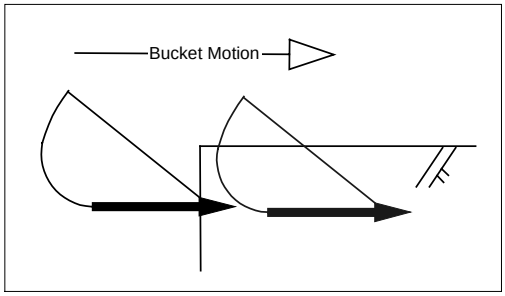

Picture 1

Picture 2

Picture 3

Picture 4

Picture 5

Figure 5.17 Small-Scale Excavation Experiment for Digging Mode II and IV

5.5.1 Digging Mode I: Separation

Digging mode I in Figure 5.18 represents a group of digging actions, which represent cases where a bucket breaks soil by relying on a main separation plate through only a separation mechanism. One of the essential requirements for a digging action to be in the digging mode I is that the bucket moves in the direction normal to the separation plate so that the bucket teeth are not engaged in any penetrating action. Therefore penetration-related resisting forces are not observed in this situation.

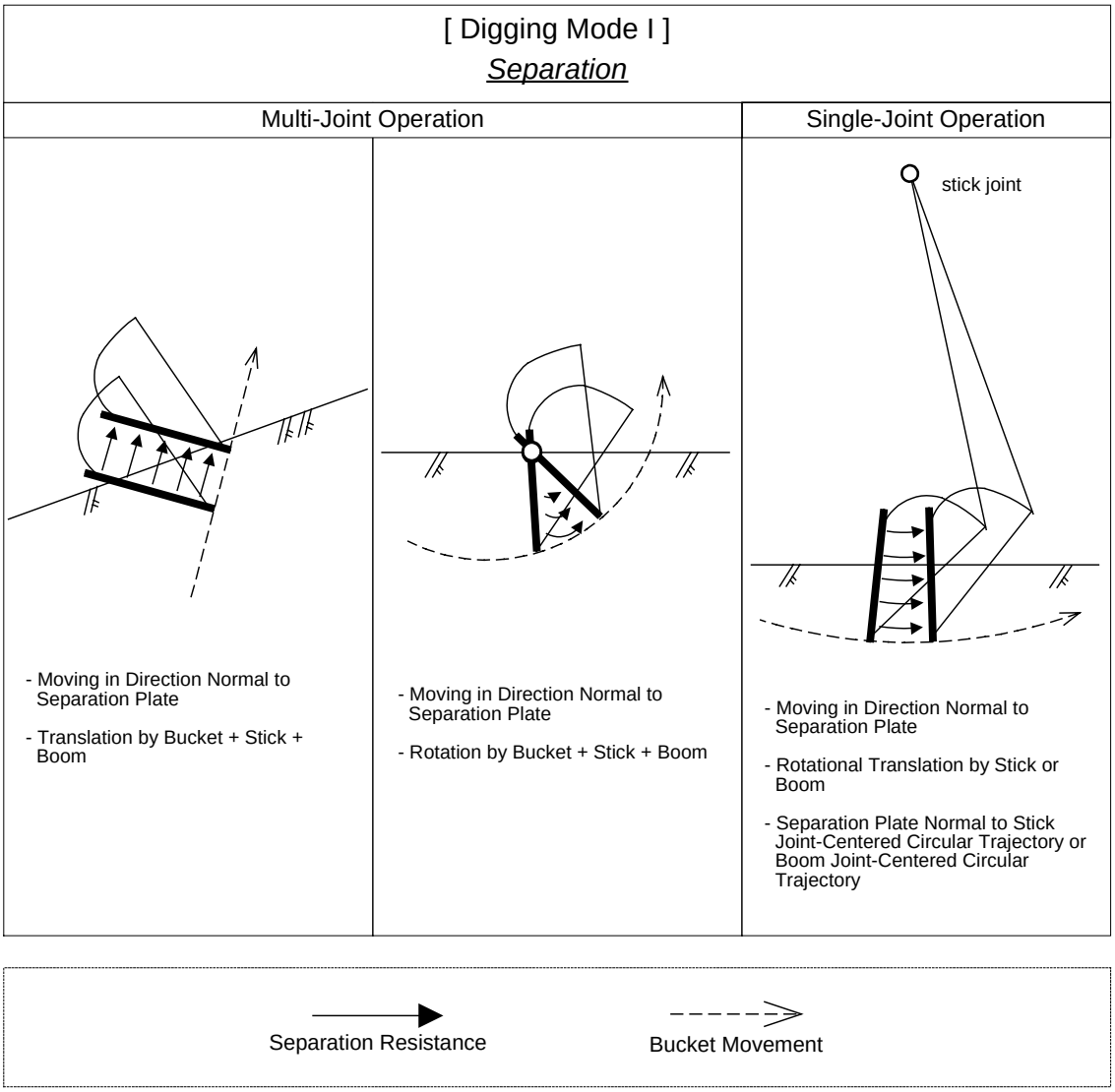

Figure 5.18 Digging Mode I: Separation

Depending upon driver's operations, however, there are different motional transformations of a separation plate. The first case in Figure 5.18 shows a situation where a bucket makes a linear translation while maintaining its direction normal to a separation plate. This digging motion can be achieved by simultaneously operating multiple joints for a bucket, a stick and a boom.

The second case is when a bucket rotates itself against an arbitrary point along in a separation plate. Even though it is rotational transformation, it meets the requirement that every point in the separation plate maintains a normal angle to the separation plate in its moving trajectory. Since the rotational point is not one of the mechanical joints, this motion can be realized by manipulating a bucket, a stick and a boom together.

The last case in Figure 5.18 represents a single joint operation using either a stick joint or a boom joint. While a bucket makes a stick joint-centered or a boom joint-centered circular trajectory, the separation plate maintains a normal angle to the trajectory and does not introduce penetration resistance.

5.5.2 Digging Mode II: Penetration

Figure 5.19 shows another single-mechanism mode, where bucket teeth play a major role to penetrate into soil media and a separation plate creates some adhesion and friction as described in the previous section. Unlike digging mode I, the direction of a bucket movement is tangential to the separation plate and the teeth. Therefore, in this digging mode, separation-related resisting forces are non-existent.

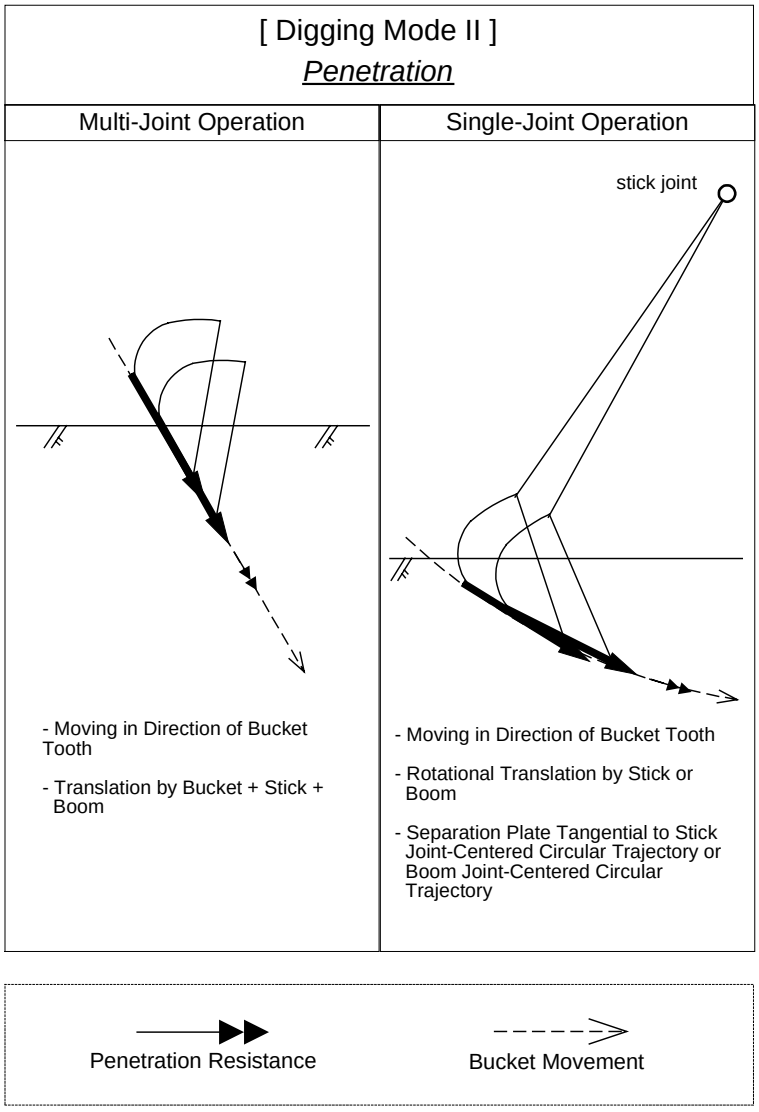

Figure 5.19 Digging Mode II: Penetration

The first case represents a digging operation, in which bucket teeth makes a linear translation while meeting the tangent condition along the moving direction. This action is possible by operating multiple joints of a bucket, a joint and a boom.

The second case shows a single-joint operation by moving either only a stick or a boom. Even though the bucket is not making linear translation but circular trajectory, as long as the teeth keep tangential contact with the trajectory, any operation of this type can be classified as digging mode II.

5.5.3 Digging Mode III: Separation and Penetration

Digging mode III in Figure 5.20 is a group of multi-mechanism-based digging actions, where separation and penetration resisting forces are generated by the interaction between soil and a separation plate and bucket teeth. This digging mode is in between digging mode I and II in that the angle a separation plate and teeth form with the direction of bucket movement is theoretically an arbitrary angle between $0 \sim 90^{o}$. As a result, there are separation as well as penetration resisting forces existent in this digging mode.

The first case shows a situation where a bucket moves in linear fashion with a separation plate and teeth angled with the linear trajectory. The linear movement is broken down into a normal component for separation resistance and a tangential component for penetration resistance. This action can be made using multiple joints.

The second case is a single-joint operation using a bucket joint, where the trajectory of a bucket tip is circular in shape. In this case, a separation plate and teeth always forms an acute angle with the trajectory.

The third case is another single-joint operation through either a stick joint or a boom joint. In this case a separation plate and teeth needs to maintain an acute angle with a circular trajectory.

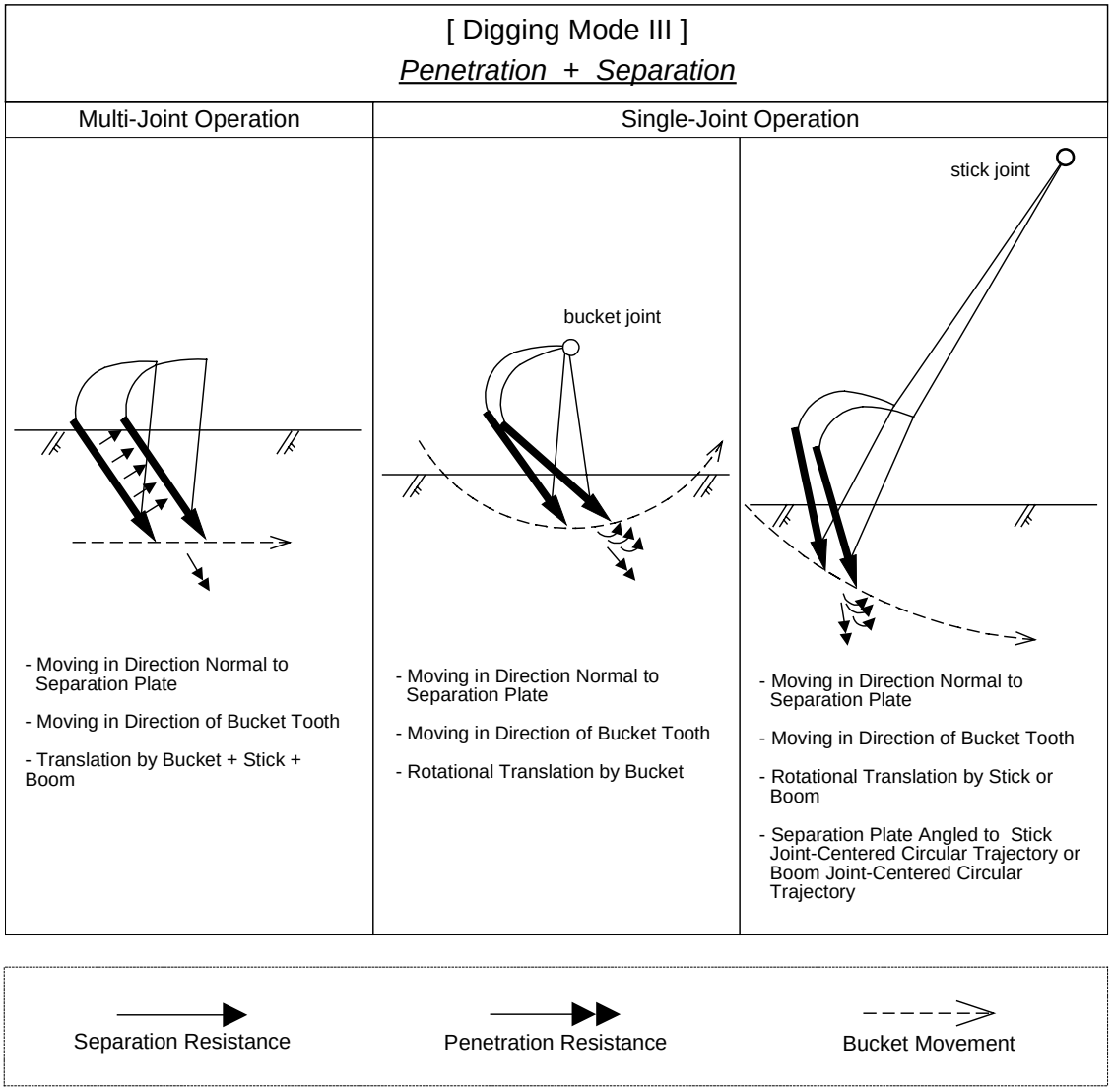

Figure 5.20 Digging Mode III: Separation + Penetration

5.5.4 Digging Mode IV: Penetration and Secondary Separation

Digging mode IV is another group of multi-mechanism digging actions, where penetration and secondary separation resisting forces are induced by bucket teeth and a secondary separation plate. As far as motional requirements are concerned, this digging mode is exactly the same as digging mode II. This mode differs from mode II in that a bucket in this mode needs to be embedded deep enough in soil media so that secondary separation resistance can be generated by a secondary separation plate as shown in Figure 5.21.

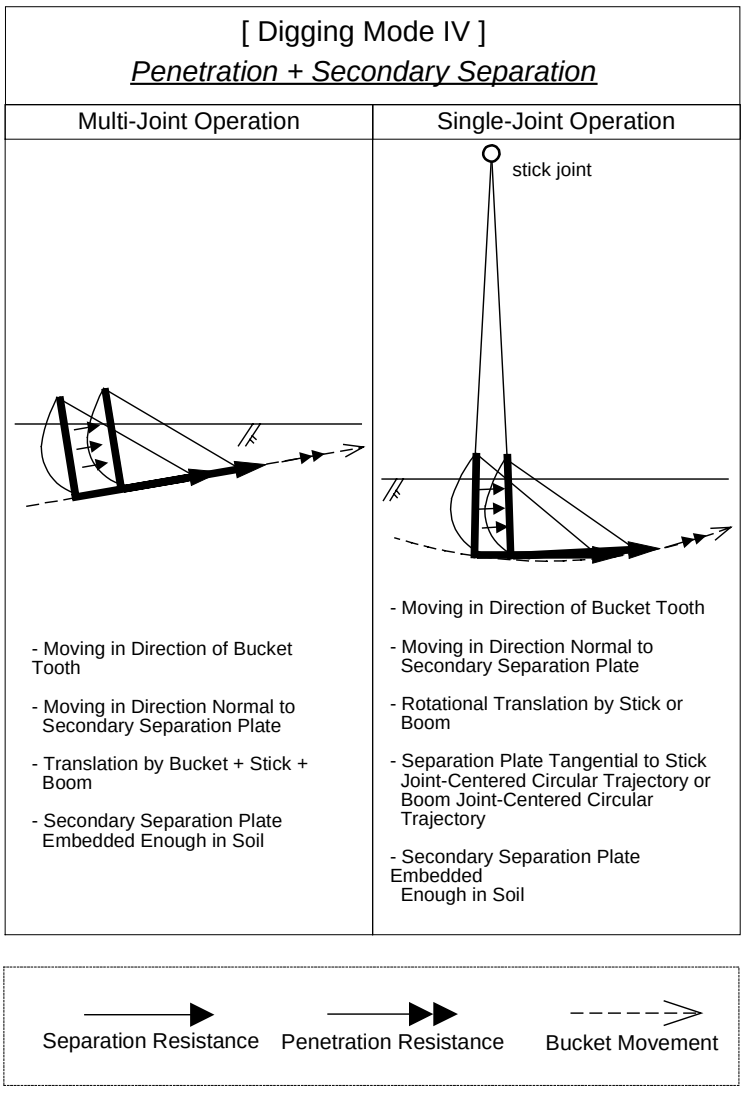

Figure 5.21 Digging Mode IV: Penetration + Secondary Separation

5.5.5 Digging Mode V: Penetration, Separation and Secondary Separation

Digging mode V in Figure 5.22 is the last group of digging actions, where separation, penetration and secondary separation resisting forces are generated by a separation plate, teeth and a secondary separation plate. Digging mode V is an extended version of digging mode III in that this digging mode uses the same motional and angle requirements as digging mode III does and requires one more requirement that a bucket needs to be embedded in soil enough for a secondary separation plate to function as a source of secondary separation resistance.

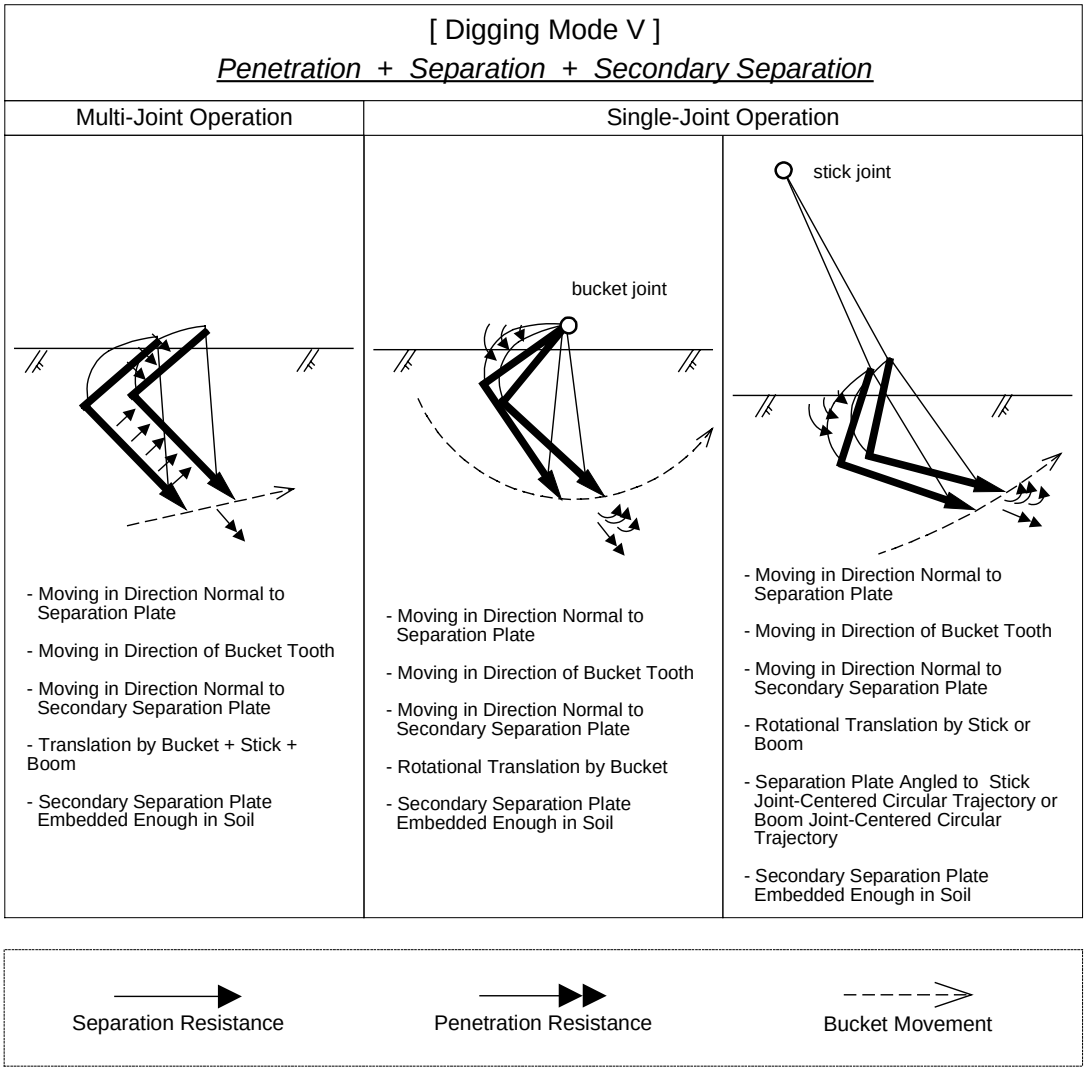

Figure 5.22 Digging Mode V: Penetration + Separation + Secondary Separation

5.6 Conclusion

The mathematical model of excavator digging (or physics-based soil model of excavator digging) consists of many elements to predict soil resistance forces in an excavator digging process. Those elements are as follows.

1) Soil resistance models:
    a. Generalized separation model
    b. Penetration model
2) Excavator digging modes

The idea is that any excavator digging action with a short time span is classified into one of digging modes using the specified requirements to identify its underlying digging mechanisms. Based upon the identification, either the generalized separation model, the penetration model or both are used to predict resisting forces for each mechanism and to form a total resistance by combining each resistance force. These calculated resistance forces are used by the simulation engine when they are compared with the bucket forces calculated from the excavator computational model (or physics-based excavator model). Therefore, the behavior of an excavator bucket engaged in soil digging is controlled properly in a physically meaningful way.

The description in this chapter, however, is not limited only to the development of the VR excavator simulator system. The information is general enough to be used in other applications. For example, an optimum digging operation practice can be determined by comparing different resistance profiles for different operation cases and selecting the one with the least amount of soil resistance.